View metadata, citation and similar papers at core.ac.uk

brought to you by CORE

provided by Elsevier - Publisher Connector

NEOPLASIA
www.neoplasia.com

Volume 14 Number 2 February 2012 pp. 150–158 150

The Brain Microenvironment Preferentially Enhances the Radioresistance of CD133$^+$ Glioblastoma Stem-like Cells

Muhammad Jamal, Barbara H. Rath, Patricia S. Tsang, Kevin Camphausen and Philip J. Tofilon

Radiation Oncology Branch, National Cancer Institute, National Institutes of Health, Bethesda, MD, USA

Abstract

Brain tumor xenografts initiated from glioblastoma (GBM) CD133$^+$ tumor stem-like cells (TSCs) are composed of TSC and non-TSC subpopulations, simulating the phenotypic heterogeneity of GBMs *in situ*. Given that the discrepancies between the radiosensitivity of GBM cells *in vitro* and the treatment response of patients suggest a role for the microenvironment in GBM radioresistance, we compared the response of TSCs and non-TSCs irradiated under *in vitro* and orthotopic conditions. As a measure of radioresponse determined at the individual cell level, γH2AX and 53BP1 foci were quantified in CD133$^+$ cells and their differentiated (CD133$^-$) progeny. Under *in vitro* conditions, no difference was detected between CD133$^+$ and CD133$^-$ cells in foci induction or dispersal after irradiation. However, irradiation of orthotopic xenografts initiated from TSCs resulted in the induction of fewer γH2AX and 53BP1 foci in CD133$^+$ cells compared to their CD133$^-$ counterparts within the same tumor. Xenograft irradiation resulted in a tumor growth delay of approximately 7 days with a corresponding increase in the percentage of CD133$^+$ cells at 7 days after radiation, which persisted to the onset of neurologic symptoms. These results suggest that, although the radioresponse of TSCs and non-TSCs does not differ under *in vitro* growth conditions, CD133$^+$ cells are relatively radioresistant under intracerebral growth conditions. Whereas these findings are consistent with the suspected role for TSCs as a determinant of GBM radioresistance, these data also illustrate the dependence of the cellular radioresistance on the brain microenvironment.

Neoplasia (2012) 14, 150–158

Introduction

Whereas radiotherapy significantly prolongs the survival of patients with glioblastoma (GBM), most patients die of their disease within 1 to 2 years of diagnosis [1]. Because most GBMs recur in the initial treatment volume [2] and because an increase in total dose fails to improve local control [3], these tumor cells *in situ* are considered to be radioresistant. Thus, a strategy for improving GBM therapeutic response is to delineate the mechanisms mediating this radioresistance, which should then aid in the development of target-based radiosensitizers. Toward this end, most preclinical investigations of GBM radioresponse have used long-established glioma cell lines. However, in both *in vitro* and *in vivo* characteristics, these cell lines have little in common with GBM *in situ* [4]. Data now suggest that GBMs are driven and maintained by a subpopulation of clonogenic cells referred to as tumor stem-like cells (TSCs) [5,6]. The putative role of TSCs in GBM biology suggests that this tumor cell subpopulation also serves as a source of GBM radioresistance.

As a test of this scenario, Bao et al. [7] used a clonogenic assay to compare the *in vitro* radiosensitivity of GBM TSC lines as identified by CD133 expression and CD133$^-$ non-TSCs isolated from the same tumor specimen or xenograft. Although radiation survival curves were not provided, representative images showed fewer colonies after irradiation with 5 Gy in CD133$^-$ cultures compared with CD133$^+$ cultures, consistent with TSC radioresistance [7]. The resistance of CD133$^+$ cells was then attributed to an enhanced capacity to repair radiation-induced DNA damage [7] as determined by the alkaline comet assay, which measures DNA single-strand breaks [7,8], and γH2AX foci dispersal, which reflects the repair of DNA double-strand breaks (DSBs) [9]. On the basis of these initial results, TSCs have been assumed to provide an *in vitro* model for defining the mechanisms of resistance and the testing of novel

Address all correspondence to: Philip J. Tofilon, PhD, Radiation Oncology Branch, National Cancer Institute, 10 Center Dr, MSC 1002, Building 10, B3B69B, Bethesda, MD 20892. E-mail: tofilonp@mail.nih.gov

Received 22 December 2011; Revised 26 January 2012; Accepted 30 January 2012

Copyright © 2012 Neoplasia Press, Inc. All rights reserved 1522-8002/12/$25.00
DOI 10.1593/neo.111794

GBM treatment strategies. However, the clinical relevance of TSCs as an experimental model depends on whether they actually simulate therapeutic response of GBM *in situ*. With respect to radiotherapy, this does not seem to be the case. TSCs are considerably more radiosensitive than long-established glioma cell lines as defined by clonogenic analysis; the enhanced sensitivity of TSCs was associated with a relative defect in DNA DSB repair [10]. Moreover, categorizing TSCs isolated from GBM specimens as radioresistant *versus* other subpopulations is complicated by the experimental difficulties in generating radiation cell survival curves for both the clonogenic TSC and their non-TSC counterparts. Along these lines, recent studies showed no difference between CD133$^+$ TSCs and their CD133$^-$ differentiated progeny in DNA repair capacity [11,12], a critical determinant of radiosensitivity, suggesting that the relative radioresistance of TSCs may be cell line dependent. Thus, as defined by *in vitro* analyses, the significance of TSCs as a source of GBM radioresistance is unclear.

Whereas GBMs are characterized by extensive intertumor heterogeneity, the brain microenvironment is common to all GBMs. To determine the influence of the orthotopic environment on the intrinsic radiosensitivity of GBM cells, we recently used γH2AX foci to directly compare the radioresponse of GBM TSCs grown *in vitro* and as intracerebral (IC) xenografts [11]. Induction of γH2AX foci corresponds to radiation-induced DNA DSBs and their dispersal correlates with DSB repair [13,14]. Because DSBs are the critical lesion in radiation-induced cell death, γH2AX foci can provide a measure of radiosensitivity [15–17]. For two TSC lines, the initial level of radiation-induced γH2AX foci was found to be significantly reduced in tumor cells within IC xenografts and the foci that did form dispersed more rapidly compared with cells irradiated under the *in vitro* conditions [11]. These results thus implied that GBM cells grown IC are less susceptible to DSB induction and have an increased capacity to repair DSBs, which then suggests that the brain microenvironment contributes to GBM radioresistance.

The IC implantation of CD133$^+$ TSCs results in the formation of a phenotypically heterogeneous tumor, which includes CD133$^+$ and CD133$^-$ cells in various proportions as a function of the time after implant [11]. In our initial analysis, no distinction in γH2AX foci expression was made between the cell subpopulations existing within the orthotopic xenografts. In the study presented here, we tested the hypothesis that the radiosensitivity of CD133$^+$ and CD133$^-$ cells is differentially regulated by the brain microenvironment. Toward this end, we have used dual-label immunofluorescence to compare the γH2AX and 53BP1 foci induction in CD133$^+$ *versus* CD133$^-$ cells within irradiated brain tumor xenografts.

Materials and Methods

GBM TSC Culture

The neurosphere-forming cultures NSC11 [18] (kindly provided by Dr Frederick Lang, MD Anderson Cancer Center) and GBMJ1 [10] were isolated from human GBM surgical specimens as described previously. Neurospheres were maintained in medium consisting of Dulbecco's modified Eagle medium (DMEM)/F-12 (Invitrogen, Carlsbad, CA), B27 supplement (1×; Invitrogen), and human recombinant basic fibroblast growth factor and epidermal growth factor (50 ng/ml each; R&D Systems, Minneapolis, MN). All cultures were maintained at 37°C in an atmosphere of 5% CO_2/7% O_2 [19]. CD133$^+$ cells were isolated from each neurosphere cultures by FACS [10] and used as a source for the described experiments. Both CD133$^+$ cell cultures met the criteria for TSCs [5], including self-renewal, differentiation along glial and neuronal pathways, expression of stem cell–related genes, and formation of brain tumors when implanted in immunodeficient mice [10,11].

For use in an *in vitro* experiment, CD133$^+$ neurosphere cultures were disaggregated into single cells and seeded into laminin-coated tissue culture slides as described by Hall et al. [20] in stem cell growth media. Under these conditions, the TSCs grow as an adherent monolayer, maintaining their CD133 expression and stem-like characteristics [21,22]. To induce differentiation, CD133$^+$ cells were exposed to medium consisting DMEM/F-12 and 10% fetal bovine serum (FBS) for 10 days. Differentiation was defined as the loss of CD133 expression and the gain of expression of GFAP and/or βIII-tubulin.

Generation of IC Xenografts

Athymic nude mice (*nu/nu*, males; Harlan Laboratories, Indianapolis, IN) 4 to 6 weeks of age were used in these studies. To implant tumor cells, mice were anesthetized using isoflurane gas and placed in a small animal stereotactic apparatus (Stoelting, Wood Dale, IL). Neurospheres were dissociated into single cells as previously described [10]; 10^5 CD133$^+$ cells were then injected in a total volume of 5 μl at 1.0 mm anterior and 2.0 mm lateral to the bregma to a depth of 3.5 mm at a rate of approximately 1 μl/min. Mice were observed every day until the onset of neurologic symptoms (morbidity). All experiments were performed as approved by the Institutional Animal Care and Use Committee.

Irradiation

For *in vitro* experiments, CD133$^+$ TSCs in stem cell medium or after differentiation were irradiated as monolayers using XRad 320 X-irradiator (Precision X-Ray, Inc, North Branford, CT) at 320 kV and a dose rate of 289.8 cGy/min. For *in vivo* irradiation, mice were placed in well-ventilated plexiglass jigs with shielding for the entire torso of the mouse along with critical normal structures of the head (e.g., ears, eyes, neck). Irradiation was performed using XRad 320 X-irradiator (Precision X-Ray, Inc) at 320 kV x-ray and a dose rate of 289.8 cGy/min. Sham-irradiated mice served as the control group.

Immunofluorescent Analyses of γH2AX and 53BP1 Foci

For *in vitro* analyses, CD133$^+$ NSC11 and GBMJ1 were seeded onto tissue culture slides coated with laminin as described by Hall et al. [20]. To visualize foci, cultures were fixed with 4% paraformaldehyde, permeabilized with 0.1% Triton X-100, and blocked with 1% bovine serum albumin in phosphate-buffered saline (PBS) containing 5% goat serum. The slides were incubated with primary antibodies (1:1000) to phospho-H2AX (Upstate Biotechnology, Charlottesville, VA) or 53BP1 (BD Transduction Laboratories, San Jose, CA) overnight at 4°C and followed by secondary antibodies Alexa Fluor 488 goat antimouse immunoglobulin G (IgG) and Alexa Fluor 594 goat antirabbit IgG (1:1000), respectively (Molecular Probes, Eugene, OR), and mounted with Prolong Gold antifade reagent containing 4′,6-diamidino-2-phenylindole (Invitrogen) to visualize nuclei. Cells were analyzed on a Zeiss upright fluorescent microscope (Carl Zeiss MicroImaging GmbH, Jena, Germany). Data presented are the mean ± SD of three independent experiments in which 25 cells were evaluated.

For *in vivo* studies, mice were killed by CO_2 inhalation and perfused with 4% paraformaldehyde in PBS (pH 7.4) through cardiac puncture. Brains were then removed and placed in 10% buffered formalin for 48 hours before embedding in paraffin. The paraffin-embedded brains were cut into 10-μm-thick slices; sections were deparaffinized in xylene

and rehydrated in decreasing grades of alcohol. Sections were boiled in citrate buffer and incubated in 1% bovine serum albumin in PBS containing 10% goat serum. The slides were then incubated with primary antibodies to γH2AX (1:500; Upstate Biotechnology) or 53BP1 (1:500; BD Transduction Laboratories) and CD133 (1:500; Cell Signaling, Danvers, MA) overnight at 4°C followed by secondary antibodies Alexa Fluor 488 goat antimouse IgG and Alexa Fluor 594 goat antirabbit IgG at 1:500, respectively, and mounted with Prolong Gold antifade containing 4′,6-diamidino-2-phenylindole (Invitrogen) to visualize nuclei. γH2AX or 53BP1 foci were determined in CD133$^+$ and CD133$^-$ cells within the same xenograft. Foci analysis was performed using a Leica confocal microscope (Leica TCS SP5 Confocal, Mannheim, Germany) with evaluation of only nonnecrotic tumor tissue. To obtain an accurate foci count, the depth of the nuclei was scanned by focusing manually along the optical axis (*z* direction; original magnification, ×100), and images of 10 to 20 slices were recorded per *z* stack to map the entire nucleus. This procedure is necessary to prevent underscoring of foci due to incomplete visualization of the entire nucleus [17]. Data are presented as the mean ± SD of three mice collected in at least three independent experiments in which 50 cells per phenotype were evaluated. Differences between CD133$^+$ and CD133$^-$ cells were evaluated according to Student's *t* test with statistical significance defined as $P < .05$.

Generation of Luciferase-Expressing Cells and Bioluminescence Imaging

Cells were engineered to express luciferase using the lentivirus LVpFUGW-UbC-ffLuc2-eGFP2, a bimodal expression vector fused with the combination of the bioluminescent protein ffLuc2 and fluorescent protein eGFP2 under the control of the UbC promoter, provided by the Viral Technology Laboratory, Advanced Technology Program, National Cancer Institute - Frederick, MD. CD133$^+$ NSC11 cultures were disaggregated into single cells and exposed to the lentivirus for 24 hours. Transduction was monitored by GFP fluorescence; GFP$^+$ CD133$^+$ cells were isolated by FACS. The transduced CD133$^+$ NSC11 cells were then allowed to divide in neurosphere growth medium before IC implantation. Of note, after exposure to medium consisting of DMEM/F-12 and 10% FBS to induce differentiation, the transduced NSC11 cells (CD133$^-$) continued to express GFP and luciferase. To perform bioluminescence imaging (BLI), mice were injected intraperitoneally at 0.01 ml/g body weight with D-luciferin (15 mg/ml; Gold Biotechnology, St. Louis, MO). Mice were then anesthetized with isoflurane and evaluated using the Xenogen imaging system (IVIS 200; Caliper Life Sciences, Mountain View, CA). Bioluminescence was expressed as total photons per second using Living Image software version 3.1 (Caliper Life Sciences). Data are presented as the mean ± SE of eight to nine mice per group.

Percentage of CD133$^+$ Cells in IC Xenograft Tumors

Paraffin-embedded brains from specified treatment groups were cut into 6-μm-thick slices and stained for CD133 as described above. The percentage of CD133-positive cells within IC xenografts was calculated in nonnecrotic, healthy areas of tumor tissue in whole section essentially as described [23]. Specifically, the percentage of CD133-positive cells was calculated by counting more than 800 cells in four or more fields selected from *x* and *y* planes at the site of IC implant at a magnification of ×40 using Leica confocal microscope. Data are presented as the mean ± SE of three to four mice per group.

Results

Radiation-Induced γH2AX Foci in NSC11 IC Xenografts: CD133$^+$ Versus CD133$^-$ Cells

To define the influence of the central nervous system microenvironment on TSC radioresponse, we first compared *in vitro* cultures of NSC11 CD133$^+$ TSCs to those of their differentiated CD133$^-$ progeny using γH2AX foci, which provides an indicator of radiation-induced DSBs [13,14]. For this analysis, CD133$^+$ NSC11 cells were maintained in stem cell medium (TSCs) or exposed to 10% FBS for 10 days (differentiated), which results in the loss of CD133 expression and differentiation along astroglial and neuronal pathways [11]. In contrast to our previous study using poly-L-lysine [11], cells were seeded onto slides coated with laminin to better approximate the neural stem cell microenvironment [20]. As previously reported, CD133$^+$ TSCs seeded onto a laminin-based matrix grow as an evenly dispersed adherent monolayer [21,22]. As shown in Figure 1*A*, the number of γH2AX foci induced as a function of radiation dose (as determined at 0.5 hours after irradiation) was essentially the same for CD133$^+$ and CD133$^-$ NSC11 cells. Moreover, the dispersal of γH2AX foci induced by 2 Gy was not significantly different between the two phenotypes (Figure 1*B*). These results suggest that, under *in vitro* conditions, the induction and repair of DSBs after irradiation of CD133$^+$ TSCs are similar to those of their CD133$^-$ differentiated progeny.

To test whether a similar relationship between the radioresponse of TSCs and their differentiated progeny exists under orthotopic conditions, we used IC xenografts initiated from NSC11 CD133$^+$ cells. In this model system, although the initial IC implant is of 100% CD133$^+$ cells, xenografts at the time of morbidity are composed of a variety of cell subpopulations including those expressing GFAP or βIII-tubulin [11], which is consistent with tumor cells that have differentiated, at least partially, along astrocytic and neuronal pathways, respectively. In addition, there continues to be a CD133$^+$ subpopulation (~10%), suggesting the presence of TSCs. This xenograft model thus simulates the phenotypic diversity found in GBMs in a clinical setting; moreover, it allows for the direct comparison of the radioresponse of CD133$^+$ and CD133$^-$ cells under the unique conditions of the brain microenvironment.

Toward this end, γH2AX foci were quantified in individual nuclei using confocal microscopy and a stacking procedure that allowed for evaluation of whole nuclei in the *z* direction for CD133$^+$ and CD133$^-$ cells within the same 10-μm section. Mice bearing NSC11 IC tumors were locally irradiated (6 Gy) at the initial onset of neurologic symptoms (morbidity) and killed at times out to 24 hours. Dual-label immunofluorescence was used to identify γH2AX foci specifically in CD133$^+$ or CD133$^-$ cells. The CD133$^+$ cells represent TSCs; the CD133$^-$ cells represent non-TSC cells that have undergone at least partial differentiation. Only tumor cells in nonnecrotic regions of the tumor mass were evaluated (Figure 2*A*). Representative composite images of γH2AX foci in CD133$^+$ and CD133$^-$ cells in NSC11 xenografts are shown in Figure 2*B*.

γH2AX foci were quantified in each phenotype within a xenograft as a function of time after irradiation (Figure 2*C*). For CD133$^+$ and CD133$^-$ cells, the number of γH2AX foci reached a maximum at 0.5 hours after irradiation followed by a rapid decline at 1 hour with a further reduction by 6 hours. There was no further reduction in foci number between 6 and 24 hours in either phenotype, although CD133$^-$ cells remained above control at 24 hours. Whereas the time course of γH2AX foci dispersal was similar between phenotypes, the

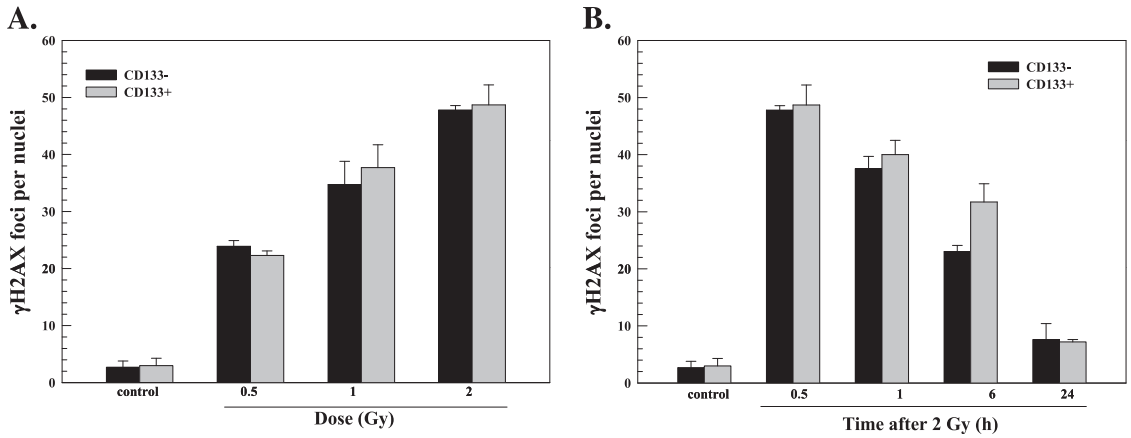

Figure 1. γH2AX foci after irradiation of NSC11 cells *in vitro*. Monolayer cultures of CD133$^-$ cells (black bars) or CD133$^+$ cells (gray bars) were irradiated and analyzed 0.5 hours later (A) or irradiated with 2 Gy and analyzed at the specified times (B). Values shown represent the mean ± SD of three independent experiments in which 25 cells were scored. The 2-Gy/0.5-h value is repeated in A and B.

number of γH2AX foci in CD133$^-$ cells at 0.25 and 0.5 hours was dramatically elevated over the number induced in CD133$^+$ cells. To better illustrate the difference in initial γH2AX induction, the dose response for CD133$^+$ and CD133$^-$ cells at 0.5 hours after irradiation is shown in Figure 2*D*. At each dose tested, the number of γH2AX foci induced in CD133$^-$ cells was more than that induced in CD133$^+$ cells with the difference at 4 and 6 Gy reaching statistical significance. In contrast to NSC11 cells grown *in vitro* (Figure 1), these results indicate that CD133$^+$ cells within orthotopic xenografts were significantly less susceptible to γH2AX foci induction, which suggests that they are less susceptible to radiation-induced DSBs. Although at 24 hours γH2AX foci levels remained above control for CD133$^-$ but not CD133$^+$ cells, given the substantially larger number of foci induced in the CD133$^-$ cells, it is difficult to determine whether this reflects a relative defect in foci dispersal and thus DSB repair capacity. Of note, whereas more γH2AX foci were induced in CD133$^-$ cells than in CD133$^+$ cells within xenografts, the CD133$^-$ cells irradiated under orthotopic conditions were substantially less susceptible to γH2AX induction than NSC11 cells (CD133$^+$ and CD133$^-$) irradiated *in vitro* (Figure 1 *vs* Figure 2, *C* and *D*). These results are consistent with the overall reduction in the susceptibility to radiation-induced DSBs of NSC11 cells grown as IC xenografts compared with *in vitro* [11].

Radiation-Induced 53BP1 Foci in NSC11 IC Xenografts: CD133$^+$ Versus *CD133$^-$ Cells*

53BP1 protein is a component of the DNA damage response network that also forms nuclear foci in response to ionizing radiation [24]. The retention of 53BP1 at nuclear foci is facilitated by γH2AX, yet its initial recruitment to the site of DSBs does not require γH2AX [25] and thus provides an independent measure of DSB induction [17,25]. Analysis of NSC11 CD133$^+$ and their differentiated (CD133$^-$) progeny grown *in vitro* on laminin showed no significant difference between the phenotypes in the 53BP1 foci induction as a function of radiation dose or dispersal after 2 Gy (Figure 3). As for γH2AX, analysis of radiation-induced 53BP1 foci was then extended to CD133$^+$ and CD133$^-$ cells within brain tumor xenografts initiated from NSC11 CD133$^+$ cells. Representative composite images of 53BP1 foci in CD133$^+$ and CD133$^-$ cells within NSC11 IC xenografts are shown in Figure 4*A*. In both phenotypes, 53BP1 foci dispersed rapidly between 0.5 and 1 hour after irradiation approaching control levels by 6 hours (Figure 4*B*). As for γH2AX, the number of 53BP1 foci in CD133$^-$ cells at 0.5 hours after irradiation was significantly greater than in CD133$^+$ cells. These results indicate that, under orthotopic growth conditions, CD133$^+$ cells are less susceptible to 53BP1 foci formation, which further suggests that cells expressing this TSC marker are relatively less susceptible to radiation-induced DSBs.

Radiation-Induced Nuclear Foci in GBMJ1 IC Xenografts: CD133$^+$ Versus *CD133$^-$ Cells*

To determine whether these results were unique to NSC11 tumors, similar experiments were performed using the TSC line GBMJ1. The orthotopic implantation of GBMJ1 CD133$^+$ cells results in the formation of phenotypically heterogeneous brain tumors composed of cells expressing GFAP, βIII-tubulin, and CD133 [11]. At the initial onset of neurologic symptoms, the xenografts consisted of approximately 10% CD133$^+$ cells [11]. After local irradiation (6 Gy), γH2AX foci were readily detectable at 0.5 hours in CD133$^+$ and CD133$^-$ cells, returning to unirradiated levels by 6 hours in both phenotypes (Figure 5*A*). However, at 0.5 and 1 hour after irradiation, there were significantly fewer γH2AX foci in CD133$^+$ cells compared with CD133$^-$ cells. Similar results were obtained for 53BP1 foci induction (Figure 5*B*). That is, the number of 53BP1 foci induced at 0.5 hours after irradiation was significantly less in CD133$^+$ cells than in CD133$^-$ cells. Thus, in orthotopic xenografts initiated from GBMJ1 TSCs, CD133$^+$ cells were less susceptible to radiation-induced γH2AX and 53BP1 foci formation than CD133$^-$ cells. To determine whether there was a similar differential in the initial level of foci induction *in vitro*, γH2AX and 53BP1 foci were quantified at 0.5 hours after irradiation of GBMJ1 CD133$^+$ cells and their differentiated CD133$^-$ progeny grown in monolayer culture (Figure 5, *C* and *D*). As for NSC11 cells, under *in vitro* growth conditions, no difference in γH2AX or 53BP1 foci induction was detected between GBMJ1 CD133$^+$ cells and CD133$^-$ cells. These results suggest that, in contrast to *in vitro* conditions, CD133$^+$ cells in GBMJ1 tumors are less susceptible to radiation-induced DSB formation compared with CD133$^-$ cells, again implicating the brain microenvironment as a source of the differential response between phenotypes. In addition, whereas more foci were induced in CD133$^-$ cells than CD133$^+$ cells within GBMJ1 xenografts, the

number of foci induced in CD133$^-$ cells irradiated under orthotopic conditions at 0.5 hours after 6 Gy was in the same range as that induced in GBMJ1 cells (CD133$^-$ and CD133$^+$) *in vitro* after 2 Gy (Figure 5, *A* and *B vs C* and *D*). These results are consistent with the overall reduction in the susceptibility to radiation-induced DSBs of GBMJ1 cells grown as IC xenografts compared with *in vitro* [11].

Percentage of CD133$^+$ Cells within Irradiated NSC11 Xenografts

The data presented here suggest that CD133$^+$ cells within orthotopic xenografts are relatively radioresistant compared with CD133$^-$ cells. If this is the case, then the percentage of CD133$^+$ cells should increase as a function of time after irradiation. To test this hypothesis, we first

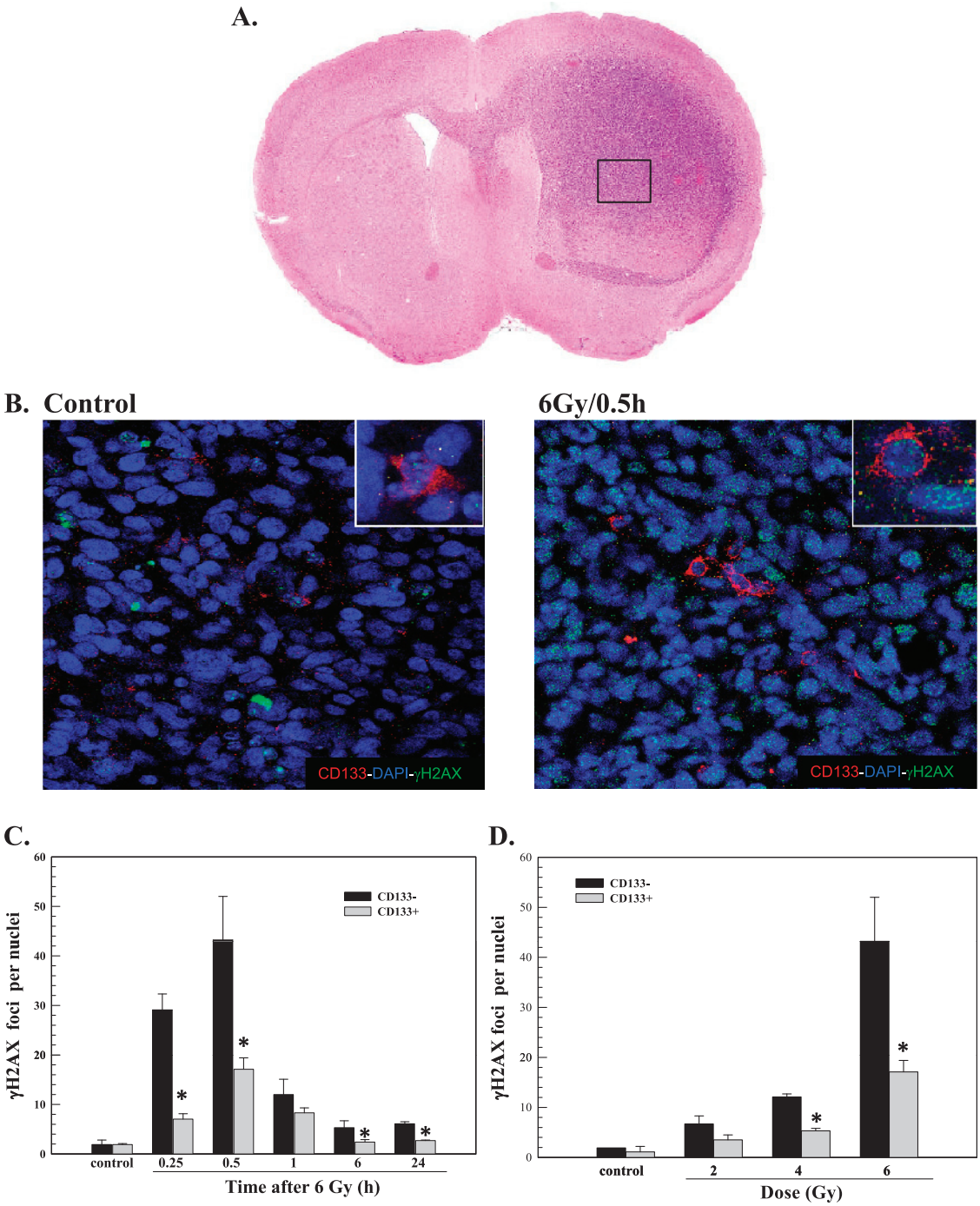

Figure 2. γH2AX foci in CD133$^-$ and CD133$^+$ cells after irradiation of IC xenografts initiated from NSC11 TSCs. IC xenografts initiated from CD133$^+$ NSC11 cells were locally irradiated (6 Gy) at the initial signs of morbidity. (A) Hematoxylin and eosin staining of representative tumor-bearing mouse brain; the box illustrates the general tumor area evaluated in immunofluorescent analyses. (B) Representative maximum projection confocal micrographs (magnification, ×40; inserts, ×63) of γH2AX nuclear foci (green), CD133$^+$ cells (red), and nuclei (blue) within IC tumor xenografts. (C) γH2AX foci induction and dispersal within CD133$^-$ (black bars) and CD133$^+$ cells (gray bars) after irradiation of IC xenografts. (D) γH2AX foci induced at 0.5 hours as a function of radiation dose for CD133$^-$ (black bars) and CD133$^+$ cells (gray bars); the 6-Gy value is the same as shown in C. Values shown represent the mean ± SD for three mice in which 50 tumor cells per phenotype (CD133$^+$ and CD133$^-$ cells) were scored within the same xenograft. *$P < .05$ for CD133$^+$ *versus* CD133$^-$ cells.

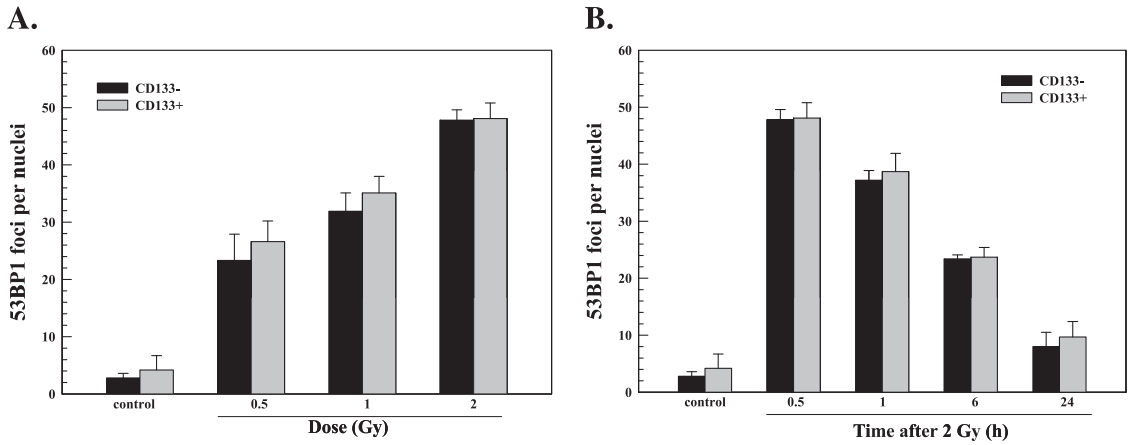

Figure 3. 53BP1 foci after irradiation of NSC11 cells *in vitro*. Monolayer cultures of CD133$^-$ cells (black bars) or CD133$^+$ cells (gray bars) were irradiated and analyzed 0.5 hours later (A) or irradiated with 2 Gy and analyzed at the specified times (B). Values shown represent the mean ± SD of three independent experiments in which 25 cells were scored. The 2-Gy/0.5-h value is repeated in A and B.

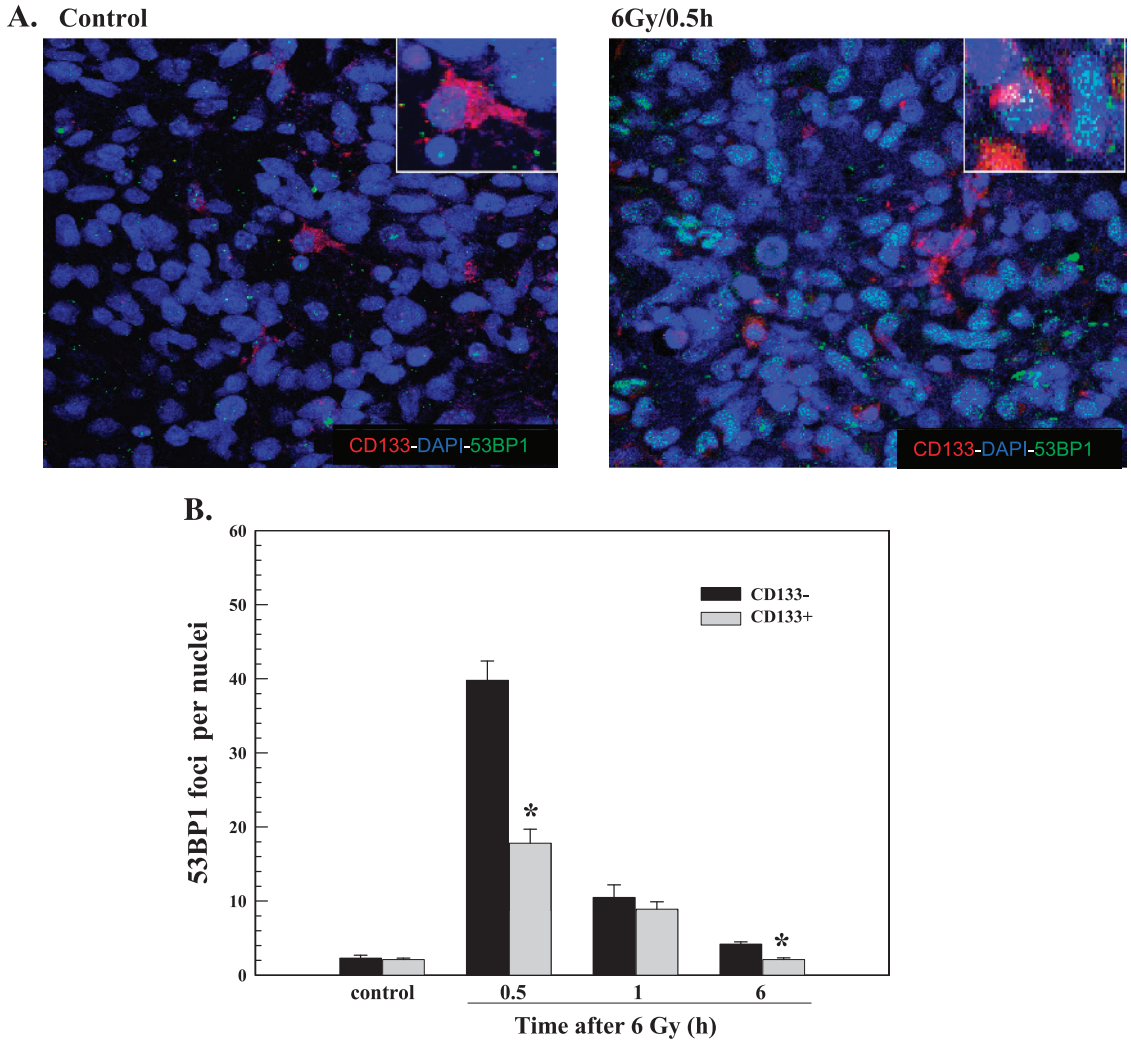

Figure 4. 53BP1 foci in CD133$^-$ and CD133$^+$ cells after irradiation of (IC) xenograft tumors initiated from NSC11 TSCs. IC xenografts initiated from CD133$^+$ NSC11 cells were locally irradiated (6 Gy) at the initial signs of morbidity. (A) Representative maximum projection confocal micrographs (magnification, ×40; insert, ×63) of 53BP1 nuclear foci (green), CD133$^+$ cells (red), and nuclei (blue) within IC xenografts. (B) 53BP1 foci induction and dispersal within CD133$^-$ (black bars) and CD133$^+$ cells (gray bars) after irradiation of IC xenografts. Values shown represent the mean ± SD of three mice in which 50 tumor cells per phenotype (CD133$^+$ and CD133$^-$ cells) were scored within the same xenograft. *$P < .05$ for CD133$^+$ *versus* CD133$^-$ cells.

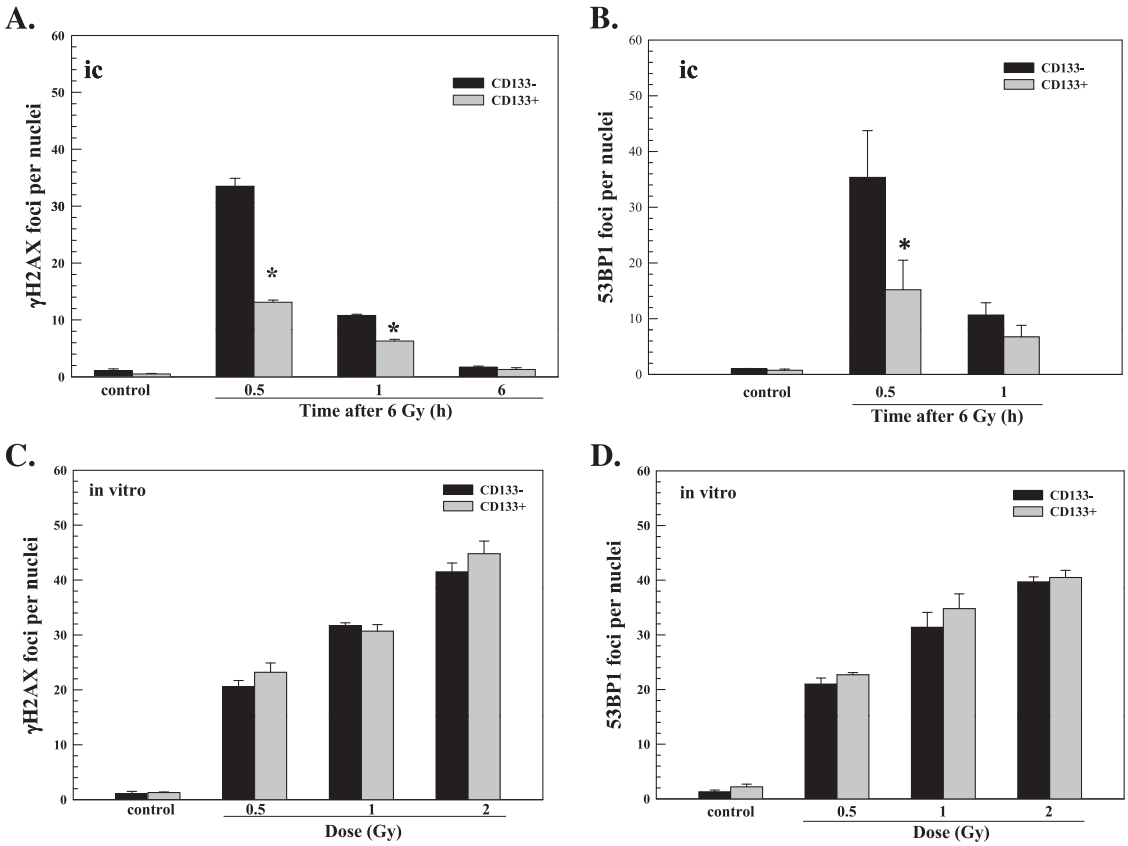

Figure 5. γH2AX and 53BP1 foci in GBMJ1 cell after *in vivo* and *in vitro* irradiation. For *in vivo* analyses, IC xenografts initiated from CD133$^+$ GBMJ1 cells were locally irradiated (6 Gy) at the initial signs of morbidity and collected for analysis at the specified times. (A) γH2AX foci in CD133$^-$ (black bars) and CD133$^+$ cells (gray bars) and (B) 53BP1 foci in CD133$^-$ (black bars) and CD133$^+$ cells (gray bars) after irradiation. Values shown represent the mean ± SD of three mice in which 50 tumor cells per phenotype (CD133$^+$ and CD133$^-$ cells) were scored within the same xenograft. For *in vitro* analyses, monolayer cultures of CD133$^-$ cells (black bars) or CD133$^+$ cells (gray bars) GBMJ1 cells were analyzed at 0.5 hours after irradiation at the specified doses: (C) γH2AX and (D) 53BP1 foci. Values shown represent the mean ± SD of three independent experiments in which 25 cells were scored. *$P < .05$ for CD133$^+$ *versus* CD133$^-$ cells.

determined the effects of radiation on the growth rate of orthotopic xenografts initiated from CD133$^+$ NSC11 TSCs. For this analysis, TSCs were engineered to express β-luciferase using lentivirus transduction (Materials and Methods) and implanted IC. Of note, CD133$^+$ TSCs *in vitro* continue to express β-luciferase after differentiation (data not shown), which is important to the BLI of tumor size because, after IC implantation, the CD133$^+$ cells proliferate and differentiate to form a phenotypically heterogeneous tumor [11]. On day 21 after implantation, the time when a clear signal was detected by BLI, mice were locally irradiated with 12 Gy. BLI was then performed weekly until the onset of morbidity, with representative images shown in Figure 6*A*. Tumor growth was estimated as the ratio of the bioluminescence detected on a specified day to that obtained on day 21 after implantation. As shown in Figure 6*B*, bioluminescence output in control mice increased exponentially out to at least day 48 when signs of morbidity began to appear. In irradiated mice, there was an initial delay of approximately 7 days, after which bioluminescence output increased at approximately the same rate as in control mice. It should be noted that, in a preliminary study, 6 Gy did not result in any IC tumor growth delay; thus, it was necessary to increase the dose to 12 Gy. However, it was not possible to use 12 Gy in the analysis of γH2AX and 53BP1 foci in that the number of foci induced at the early time points was at the level that prevented the discrimination of individual foci and an accurate counting within individual nuclei.

We then determined the percentage of CD133$^+$ cells at the time of irradiation (day 21), when the irradiated tumors began to regrow (day 28), and at morbidity. At each time point, the percentage of CD133-positive cells was determined in nonnecrotic tumor regions as described by Tamura et al. [23]. As shown in Figure 6*C*, on day 21 after implant, the time of irradiation, the percentage of CD133$^+$ cells had already declined substantially from the initial 100% in the implant suspension to approximately 68%. In untreated mice, CD133$^+$ cells continued to decline, reaching approximately 10% by the time of tumor-induced morbidity (48-49 days after implant), consistent with previous data [11]. In mice that had received radiation, the percentage of CD133$^+$ cells was significantly greater than in control mice at 28 days and at morbidity (56-62 days after implant). Whereas it is difficult to eliminate a possible effect of radiation on TSC differentiation, these results are consistent with the nuclear foci data, suggesting that, within this brain tumor xenograft model, CD133$^+$ cells are radioresistant compared with cells that do not express CD133.

Discussion

The processes and molecules mediating the radioresistance of GBM *in situ* have been the subject of considerable research with most effort focused on *in vitro* models. However, our recent study showing that GBM cells grown as IC xenografts were substantially more radioresistant

than the same cells grown *in vitro* [11] suggests that investigations into the mechanisms mediating GBM radioresponse need to take into account the brain microenvironment. Given the potential significance of TSCs in GBM biology, we have extended our initial studies to a comparison of the CD133$^+$ and CD133$^-$ cells within GBM xenografts. For this investigation, we used two CD133$^+$ cell lines isolated from GBM surgical specimens; as previously reported, these lines fit the *in vitro* criteria of TSCs [5]. Moreover, when the CD133$^+$ cells are injected IC, histologic analysis suggests that they proliferate and differentiate along astrocytic and neuronal pathways [11,18]; at the time of tumor-induced morbidity, CD133$^+$ cells comprise a minor tumor subpopulation [11]. Although additional markers of GBM TSC phenotype exist [26] and CD133 does not identify all TSCs, the behavior of CD133$^+$ cells used in this study is consistent with the behavior of GBM TSCs [27].

Under *in vitro* growth conditions, the induction and dispersion of γH2AX and 53BP1 foci after irradiation of NSC11 and GBMJ1 CD133$^+$ cells were essentially the same as in their differentiated CD133$^-$ progeny. These results suggest that the induction and repair of radiation-induced DSBs in TSCs and non-TSCs are not significantly different *in vitro*, which is consistent with previous studies performed using other *in vitro* growth conditions [11,12]. However, within the GBM xenografts initiated from the same TSC lines, there were significantly fewer radiation-induced γH2AX foci in CD133$^+$ cells than in CD133$^-$ cells. These data suggest that, in contrast to *in vitro* growth conditions, within the orthotopic environment, CD133$^+$ cells are less susceptible to DSB induction. Similar results obtained for 53BP1 foci, the formation of which does not require H2AX expression or H2AX kinases (e.g., ATM, DNA-PK), supports the relative decrease in DSB induction in CD133$^+$ cells.

Along these lines, in a murine breast tumor model, TSCs were reported to express fewer γH2AX foci at 15 minutes after irradiation compared with the non-TSC population; importantly, the TSCs were also shown to be relatively resistant to radiation-induced cell death [28]. Applying this situation to the GBM model used in the current study suggests that the CD133$^+$ cells within the IC xenografts are radioresistant compared with CD133$^-$ cells. In the breast tumor model, the reduced level of γH2AX foci induction in TSCs was detected after both *in vitro* and *in vivo* irradiation [28]; the reduced susceptibility of GBM CD133$^+$ cells to foci induction, however, was only detectable after IC irradiation. Thus, in contrast to breast tumor cells, the radioresponse of GBM TSC and non-TSC subpopulations seems to be differentially regulated by the orthotopic microenvironment. The decrease in radiation-induced γH2AX foci in breast TSCs along with their relative radioresistance has been attributed to an increased antioxidant capacity [28]. Whether the antioxidant protection of CD133$^+$ GBM cells is preferentially enhanced under IC growth conditions remains to be determined.

Foci analysis suggests that there are fewer DSBs induced in CD133$^+$ cells after irradiation of IC xenografts, which should then be accompanied by increased survival of this phenotype. In agreement with this

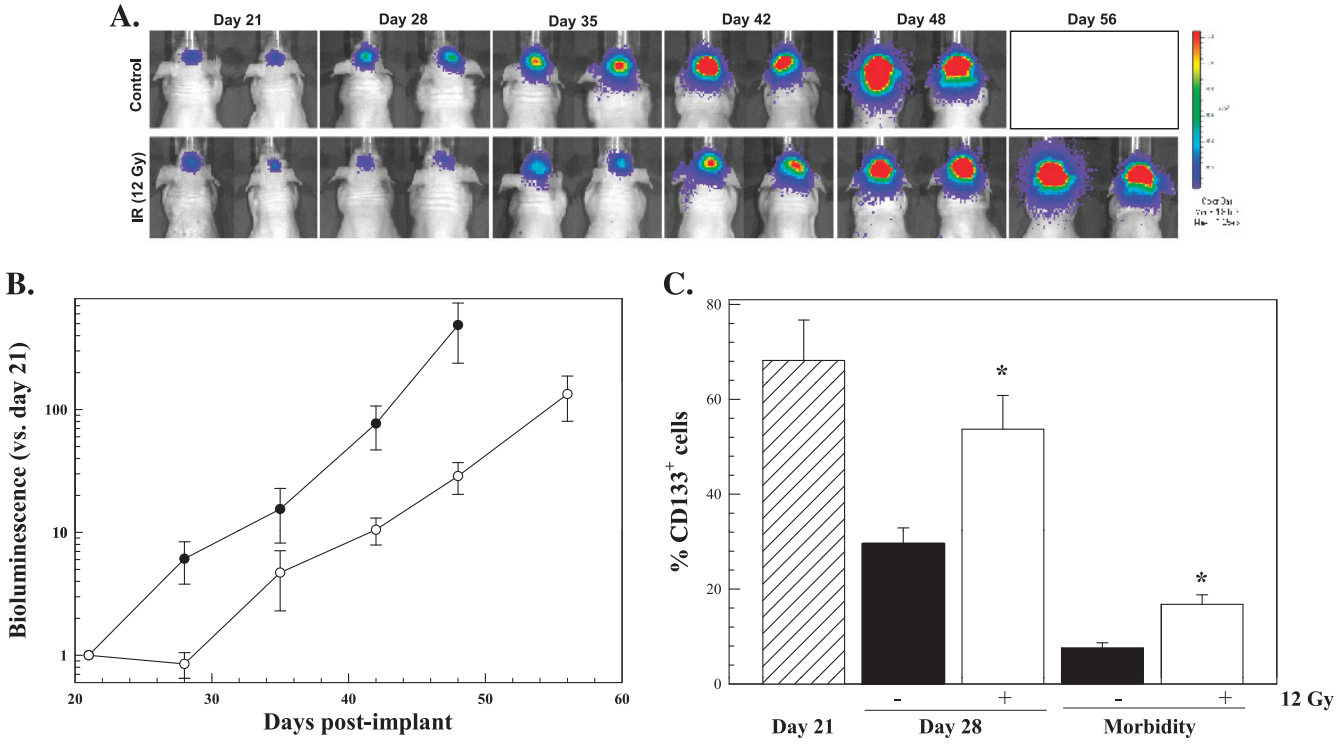

Figure 6. Influence of radiation on tumor growth and the percentage of CD133$^+$ cells within IC xenografts initiated from NSC11 TSCs. A total of 10^5 CD133$^+$ NSC11 cells were implanted IC; 21 days later, tumors were locally irradiated (12 Gy, eight mice) or sham treated (control, nine mice). (A) Representative bioluminescent images from mice bearing IC xenograft tumors initiated from CD133$^+$ NSC11 cells as a function of time after irradiation. (B) Xenograft growth estimated as the ratio of the bioluminescence output on specified days to that obtained on day 21 after implantation for control (solid circles) and irradiated (open circles) mice. Values represents the mean ± SE for eight to nine mice per group. (C) Percentage of CD133$^+$ cells in mice that did (white bars) and did not receive (black bars) radiation on day 21; hatched bar corresponds to the percentage CD133$^+$ cells on the day of irradiation. Morbidity corresponds to 48 to 49 days after implant for control mice and 56 to 62 days for irradiated mice. Values represents the mean ± SE of three to four mice per group.

putative radioresistance, the percentage of CD133$^+$ cells within irradiated xenografts was significantly increased compared with tumors that were not irradiated (Figure 6). These results are consistent with those of Tamura et al. [23] and their analysis of GBM histologic specimens obtained at the initial surgery and in a second surgery performed after high-dose radiotherapy. They showed that the percentage of CD133$^+$ cells was significantly elevated in recurrent tumors that had received high-dose radiotherapy. These results combined with xenograft studies described herein suggest that, as predicted by the tumor stem cell model, TSCs comprise a radioresistant GBM subpopulation. However, comparison to *in vitro* analyses shown here and previously [11,12] indicates that this relative radioresistance of CD133$^+$ GBM TSCs is only expressed under orthotopic conditions. Thus, these results further emphasize the significance of the brain microenvironment as a determinant of GBM therapeutic response. Whereas the specific microenvironmental factors mediating TSC radioresistance remain to be determined, the rich source of growth factors, cytokines/chemokines, and other bioactive molecules provided by the normal brain stroma is likely to be involved. Finally, with respect to preclinical studies aimed at developing clinically relevant radiosensitizers for GBM treatment, these data suggest that, for targeting the radioresistant TSC subpopulation, it will be necessary to account for the brain microenvironment.

References

[1] Stupp R, Mason WP, van den Bent MJ, Weller M, Fisher B, Taphoorn MJ, Belanger K, Brandes AA, Marosi C, Bogdahn U, et al. (2005). Radiotherapy plus concomitant and adjuvant temozolomide for glioblastoma. *N Engl J Med* **352**, 987–996.

[2] Hochberg FH and Pruitt A (1980). Assumptions in the radiotherapy of glioblastoma. *Neurology* **30**, 907–911.

[3] Chan JL, Lee SW, Fraass BA, Normolle DP, Greenberg HS, Junck LR, Gebarski SS, and Sandler HM (2002). Survival and failure patterns of high-grade gliomas after three-dimensional conformal radiotherapy. *J Clin Oncol* **20**, 1635–1642.

[4] Li A, Walling J, Kotliarov Y, Center A, Steed ME, Ahn SJ, Rosenblum M, Mikkelsen T, Zenklusen JC, and Fine HA (2008). Genomic changes and gene expression profiles reveal that established glioma cell lines are poorly representative of primary human gliomas. *Mol Cancer Res* **6**, 21–30.

[5] Singh SK, Hawkins C, Clarke ID, Squire JA, Bayani J, Hide T, Henkelman RM, Cusimano MD, and Dirks PB (2004). Identification of human brain tumour initiating cells. *Nature* **432**, 396–401.

[6] Salmaggi A, Boiardi A, Gelati M, Russo A, Calatozzolo C, Ciusani E, Sciacca FL, Ottolina A, Parati EA, La Porta C, et al. (2006). Glioblastoma-derived tumorospheres identify a population of tumor stem-like cells with angiogenic potential and enhanced multidrug resistance phenotype. *Glia* **54**, 850–860.

[7] Bao S, Wu Q, McLendon RE, Hao Y, Shi Q, Hjelmeland AB, Dewhirst MW, Bigner DD, and Rich JN (2006). Glioma stem cells promote radioresistance by preferential activation of the DNA damage response. *Nature* **444**, 756–760.

[8] Olive PL (1999). DNA damage and repair in individual cells: applications of the comet assay in radiobiology. *Int J Radiat Biol* **75**, 395–405.

[9] Rogakou EP, Pilch DR, Orr AH, Ivanova VS, and Bonner WM (1998). DNA double-stranded breaks induce histone H2AX phosphorylation on serine 139. *J Biol Chem* **273**, 5858–5868.

[10] McCord AM, Jamal M, Williams ES, Camphausen K, and Tofilon PJ (2009). CD133$^+$ glioblastoma stem-like cells are radiosensitive with a defective DNA damage response compared with established cell lines. *Clin Cancer Res* **15**, 5145–5153.

[11] Jamal M, Rath BH, Williams ES, Camphausen K, and Tofilon PJ (2010). Microenvironmental regulation of glioblastoma radioresponse. *Clin Cancer Res* **16**, 6049–6059.

[12] Ropolo M, Daga A, Griffero F, Foresta M, Casartelli G, Zunino A, Poggi A, Cappelli E, Zona G, Spaziante R, et al. (2009). Comparative analysis of DNA repair in stem and nonstem glioma cell cultures. *Mol Cancer Res* **7**, 383–392.

[13] Bonner WM, Redon CE, Dickey JS, Nakamura AJ, Sedelnikova OA, Solier S, and Pommier Y (2008). γH2AX and cancer. *Nat Rev Cancer* **8**, 957–967.

[14] Lobrich M, Shibata A, Beucher A, Fisher A, Ensminger M, Goodarzi AA, Barton O, and Jeggo PA (2010). γH2AX foci analysis for monitoring DNA double-strand break repair: strengths, limitations and optimization. *Cell Cycle* **9**, 662–669.

[15] Banath JP, MacPhail SH, and Olive PL (2004). Radiation sensitivity, H2AX phosphorylation, and kinetics of repair of DNA strand breaks in irradiated cervical cancer cell lines. *Cancer Res* **64**, 7144–7149.

[16] Klokov D, MacPhail SM, Banath JP, Byrne JP, and Olive PL (2006). Phosphorylated histone H2AX in relation to cell survival in tumor cells and xenografts exposed to single and fractionated doses of x-rays. *Radiother Oncol* **80**, 223–229.

[17] Rube CE, Grudzenski S, Kuhne M, Dong X, Rief N, Lobrich M, and Rube C (2008). DNA double-strand break repair of blood lymphocytes and normal tissues analysed in a preclinical mouse model: implications for radiosensitivity testing. *Clin Cancer Res* **14**, 6546–6555.

[18] Jiang H, Gomez-Manzano C, Aoki H, Alonso MM, Kondo S, McCormick F, Xu J, Kondo Y, Bekele BN, Colman H, et al. (2007). Examination of the therapeutic potential of Delta-24-RGD in brain tumor stem cells: role of autophagic cell death. *J Natl Cancer Inst* **99**, 1410–1414.

[19] McCord AM, Jamal M, Shankavaram UT, Lang FF, Camphausen K, and Tofilon PJ (2009). Physiologic oxygen concentration enhances the stem-like properties of CD133$^+$ human glioblastoma cells *in vitro*. *Mol Cancer Res* **7**, 489–497.

[20] Hall PE, Lathia JD, Caldwell MA, and Ffrench-Constant C (2008). Laminin enhances the growth of human neural stem cells in defined culture media. *BMC Neurosci* **9**, 71.

[21] Pollard SM, Yoshikawa K, Clarke ID, Danovi D, Stricker S, Russell R, Bayani J, Head R, Lee M, Bernstein M, et al. (2009). Glioma stem cell lines expanded in adherent culture have tumor-specific phenotypes and are suitable for chemical and genetic screens. *Cell Stem Cell* **4**, 568–580.

[22] Visnyei K, Onodera H, Damoiseaux R, Saigusa K, Petrosyan S, De Vries D, Ferrari D, Saxe J, Panosyan EH, Masterman-Smith M, et al. (2011). A molecular screening approach to identify and characterize inhibitors of glioblastoma stem cells. *Mol Cancer Ther* **10**, 1818–1828.

[23] Tamura K, Aoyagi M, Wakimoto H, Ando N, Nariai T, Yamamoto M, and Ohno K (2010). Accumulation of CD133-positive glioma cells after high-dose irradiation by gamma knife surgery plus external beam radiation. *J Neurosurg* **113**, 310–318.

[24] Schultz LB, Chehab NH, Malikzay A, and Halazonetis TD (2000). p53 binding protein 1 (53BP1) is an early participant in the cellular response to DNA double-strand breaks. *J Cell Biol* **151**, 1381–1390.

[25] Celeste A, Fernandez-Capetillo O, Kruhlak MJ, Pilch DR, Staudt DW, Lee A, Bonner RF, Bonner WM, and Nussenzweig A (2003). Histone H2AX phosphorylation is dispensable for the initial recognition of DNA breaks. *Nat Cell Biol* **5**, 675–679.

[26] Son MJ, Woolard K, Nam DH, Lee J, and Fine HA (2009). SSEA-1 is an enrichment marker for tumor-initiating cells in human glioblastoma. *Cell Stem Cell* **4**, 440–452.

[27] Beier D, Hau P, Proescholdt M, Lohmeier A, Wischhusen J, Oefner PJ, Aigner L, Brawanski A, Bogdahn U, and Beier CP (2007). CD133$^+$ and CD133$^-$ glioblastoma-derived cancer stem cells show differential growth characteristics and molecular profiles. *Cancer Res* **67**, 4010–4015.

[28] Diehn M, Cho RW, Lobo NA, Kalisky T, Dorie MJ, Kulp AN, Qian D, Lam JS, Ailles LE, Wong M, et al. (2009). Association of reactive oxygen species levels and radioresistance in cancer stem cells. *Nature* **458**, 780–783.